THE JOURNAL OF BIOLOGICAL CHEMISTRY VOL. 281, NO. 39, pp. 29141–29147, September 29, 2006

Solution Structure and Intermolecular Interactions of the Third Metal-binding Domain of ATP7A, the Menkes Disease Protein*[S]

Received for publication, April 4, 2006, and in revised form, July 5, 2006 Published, JBC Papers in Press, July 26, 2006, DOI 10.1074/jbc.M603176200

Lucia Banci[‡§], Ivano Bertini[‡§1], Francesca Cantini[‡§], Nunzia DellaMalva[‡¶], Torsten Herrmann[‖], Antonio Rosato[‡§], and Kurt Wüthrich[‖]**

*From the [‡]Magnetic Resonance Center (CERM), University of Florence, Via L. Sacconi 6, 50019 Sesto Fiorentino, Italy, [§]Department of Chemistry, University of Florence, Via della Lastruccia 3, 50019 Sesto Fiorentino, Italy, [¶]FiorGen Foundation, Via L. Sacconi 6, 50019 Sesto Fiorentino, Italy, [‖]Institut für Molekularbiologie und Biophysik, Eidgenössische Technische Hochschule Zürich, CH-8093 Zürich, Switzerland, and **Department of Molecular Biology, The Scripps Research Institute, La Jolla, California 92037*

The third metal-binding domain of the human Menkes protein (MNK3), a copper(I)-transporting ATPase, has been expressed in *Escherichia coli* and characterized in solution. The solution structure of MNK3, its copper(I)-binding properties, and its interaction with the physiological partner, HAH1, have been studied. MNK3 is the domain most dissimilar in structure from the other domains of the Menkes protein. This is reflected in a significant rearrangement of the last strand of the four-stranded β-sheet when compared with the other known homologous proteins or protein domains. MNK3 is also peculiar with respect to its interaction with the copper(I) ion, as it was found to be a comparatively weak binder. Copper(I) transfer from metal-loaded HAH1 was observed experimentally, but the metal distribution was shifted toward binding by HAH1. This is at variance with what is observed for the other Menkes domains.

Copper is an essential trace metal utilized as a cofactor in a variety of redox and hydrolytic proteins. In eukaryotes, copper-dependent metalloenzymes are found in multiple cellular locations (1). Excess copper, however, is highly toxic to most organisms (1, 2). Accordingly, a complex machinery of proteins that bind the metal ion controls the uptake, transport, sequestration, and efflux of copper *in vivo* (3–5). In particular, so-called metallochaperones, which deliver copper to specific intracellular targets, lower the activation barrier for copper transfer to their specific partners (6), thereby circumventing the significant thermodynamic overcapacity for copper chelation of the cytoplasm (7).

One of the pathways of copper transfer present in humans involves a small soluble metallochaperone, HAH1 (also known as Atox1) (8, 9), which is capable of delivering copper(I) both to the Menkes and the Wilson proteins (ATP7A and ATP7B, respectively) (3–5). The latter two proteins are membrane-bound P-type ATPases that translocate copper in the trans-Golgi network or across the plasma membrane (3–5), depending on environmental conditions (10). In fact, both proteins experience copper-regulated trafficking between the Golgi and plasma membranes (10). ATP7A and ATP7B have a long N-terminal cytosolic tail containing six putative metal-binding domains. Homologs of HAH1 and ATP7A/ATP7B are found in a large number of prokaryotic and eukaryotic organisms. The number of metal-binding domains in ATP7A/ATP7B homologs is variable, ranging from one to six, with proteins from higher eukaryotic organisms, *e.g.* mammals, having a higher number of such domains their prokaryotic (typically one or two) or yeast (two) homologs (11, 12).

NMR spectroscopy and x-ray crystallography have provided structures of various metal-binding domains in different metallation states for both metallochaperones and the partner ATPases (13–15). In some cases, the dynamic properties of the apo- and/or holoproteins have been directly probed by NMR in solution (13, 15). The interaction between the two partners is copper(I)-dependent (16, 17) and has been experimentally characterized on a per residue basis through NMR studies on the yeast and the *Bacillus subtilis* systems (18, 19). An atomic-level solution structure of the adduct formed by the yeast metallochaperone (Atx1) and the first metal-binding domain of the yeast ATPase (Ccc2a), in the presence of 1 equivalent of copper(I), has recently been determined (20).

The reasons why higher organisms have as many as six metal-binding domains are still unclear. Available studies on ATP7A or ATP7B trying to address this matter indicate some functional differentiation between the first four (counting from the N terminus) and the last two domains and suggest that the last two domains are sufficient for function (21–23). In addition, the mechanism of copper(I) transfer from HAH1 to either one of these two human ATPases is not completely elucidated. This

* This work was supported by grants from the Ministero dell'Istruzione, dell'Universitàe della Ricerca (MIUR COFIN 2005 and FIRB-RBLA032ZM7), Ente Cassa di Risparmio di Firenze (Progetto PROMELAB), the European Commission (Project UPMAN, LSHG-CT-2004-512052), and the Schweizerischer Nationalfonds (Project 3100A0-105570). The costs of publication of this article were defrayed in part by the payment of page charges. This article must therefore be hereby marked "*advertisement*" in accordance with 18 U.S.C. Section 1734 solely to indicate this fact.

[S] The on-line version of this article (available at http://www.jbc.org) contains supplemental Table S1 and Figs. S1–S5.

The atomic coordinates and structure factors (code 2G9O and 2GA7) have been deposited in the Protein Data Bank, Research Collaboratory for Structural Bioinformatics, Rutgers University, New Brunswick, NJ (http://www.rcsb.org/).

Resonance assignments for the NMR structures of apo- and copper(I)-MNK3 have been deposited in the BioMagResBank (code(s) 2G9O and 2GA7, respectively).

[1] To whom correspondence should be addressed: Magnetic Resonance Center, University of Florence, Via L. Sacconi, 6 50019 Sesto Fiorentino, Italy. Fax: 39-055-4574271; Tel.: 39-055-4574272; E-mail: ivanobertini@cerm.unifi.it.

process has been investigated through a variety of techniques, suggesting that there may be preferential interaction sites within the cytoplasmic tail of the ATPases. In particular, the second domain (24) and/or the fourth domain (17, 25) have been identified as preferential docking sites for HAH1. To obtain a detailed characterization at the atomic level of the role of the various domains in ATP7A, we have implemented a "divide-and-conquer" strategy by tackling a characterization of the structure, dynamics, metal-binding capabilities, and interaction with the protein partner, HAH1, of each individual soluble domain of the Menkes protein (26, 27). This approach enables the subsequent characterization of multidomain constructs, focusing on interdomain interactions and dynamics. With this approach, it was possible to study a three-domain construct, spanning ATP7A domains 4 to 6 (MNK456), and to obtain direct evidence that domain 4 is the entry site for copper(I) ions delivered by the partner and that the presence of copper(I) affects the reciprocal mobility of the three domains (25).

In this article a structural characterization of the apo- and copper(I)-form of the third domain of ATP7A, the Menkes protein (MNK3), is reported. The interaction of MNK3 with the partner human protein HAH1 has also been investigated. MNK3 is the most differentiated metal-binding domain in ATP7A, with an average sequence identity to the other domains of 32 ± 4% and a few peculiarities with respect to the other domains in its sequence. It was found that the MNK3 structure experiences some local structural rearrangements upon copper(I), at variance with the structure of the other MNK domains. MNK3 was a comparatively poor acceptor of copper(I) from HAH1. The present study constitutes a necessary step for the high-resolution investigation of the entire cytoplasmic tail of ATP7A.

MATERIALS AND METHODS

Protein Expression and Purification—The DNA sequence encoding MNK3, corresponding to amino acids 275–352 of ATP7A, was amplified via PCR and cloned in pET20, similar to what was previously done for other ATP7A domains (28). A C-terminal expression tag including His_6 was introduced to ease purification. For the sake of simplicity, hereafter residues are numbered from 1 to 78 rather than starting from 275. The K46V mutant was obtained from the plasmid encoding wild type (WT)[2]-MNK3 through the QuikChange (Stratagene) mutagenesis kit. *Escherichia coli* strain BL21(DE3)pLysS was used for protein expression. Cells were grown in minimal media with vitamin and metal supplements, using ampicillin and chloramphenicol for selection. All protein purification steps were carried out in an N_2 atmosphere chamber by affinity chromatography with a HiTrap 5-ml affinity column (Amersham Biosciences) previously charged with Zn^{2+}. Stable isotope enrichment (^{15}N or ^{13}C, ^{15}N) was performed by growing *E. coli* in M9 minimal medium using $(NH_4)_2SO_4$ and glucose as the nitrogen and carbon source, respectively.

For NMR experiments, apoprotein samples were reduced with excess dithiothreitol (DTT) and washed with 100 mM sodium phosphate buffer, pH 7.0. The final molar ratio of DTT to protein was typically 2–5-fold. Copper(I)-containing protein samples were prepared by incubating the apoprotein, after removal of DTT, with a slight excess of the acetonitrile complex of copper(I). Sample preparations were carried out in a N_2 atmosphere chamber, and the NMR tubes were sealed before being removed from the chamber. The final protein concentration in all samples was ~1 mM. NMR samples contained 10% (v/v) ^2H_2O for NMR spectrometer lock.

To investigate the interaction of MNK3 with HAH1, we titrated the latter protein in a solution containing apo-MNK3 and equimolar copper(I) directly in the NMR tube under N_2 atmosphere up to a 1:3 MNK3:HAH1 ratio. The concentration of MNK3 was around 0.3 mM.

NMR Experiments and Structure Calculations—NMR spectra were acquired at 298 K on Avance 900, 800, and 500 Bruker spectrometers equipped with triple resonance cryoprobes. The NMR experiments used for the assignment of backbone and aliphatic side chain resonances are summarized in supplemental Table S1. For apo-MNK3, all residues in the ATP7A domain (*i.e.* not taking into account the engineered expression tag) were assigned, with the sole exceptions of Ser-16 and Gln-29. In copper(I)-MNK3, all residues in the ATP7A domain were assigned, except His-13, Cys-14, Gln-29, and Ser-51. Resonance assignments are reported as supplemental information (Tables S2 and S3).

Structure calculations were performed with the software package ATNOS/CANDID/CYANA, using as input the amino acid sequence, the chemical shift lists, and three [^1H,^1H]NOE experiments, all recorded at 900 MHz with a mixing time of 110 ms: two-dimensional NOESY, three-dimensional ^{13}C-resolved NOESY, and three-dimensional ^{15}N-resolved NOESY. The standard protocol, with seven cycles of peak picking using ATNOS (29), NOE assignment with CANDID (30), and structure calculation with CYANA-2.1 (31), was applied. ϕ and ψ dihedral angle constraints were derived from the chemical shift index (32). In each ATNOS/CANDID cycle, the angle constraints were combined with the updated NOE upper distance constraints in the input for the subsequent CYANA-2.1 structure calculation cycle. In the seventh ATNOS/CANDID/CYANA cycle, a total of 4068 NOE cross-peaks were assigned from 4631 peaks picked in the spectra of apo-MNK3, which yielded 1456 meaningful NOE upper distance limits. A total of 2865 NOE cross-peaks were assigned from 3357 peaks picked in the spectra of copper(I)-MNK3, which yielded 1011 meaningful NOE upper distance limits.

The 30 conformers with the lowest residual target function values were subjected to restrained energy minimization with AMBER 8.0 (33). NOE and torsion angle constraints were applied with force constants of 32 kcal mol^{-1} $Å^{-2}$ and 32 kcal mol^{-1} $radians^{-2}$, respectively. The quality of the structures was evaluated using the program PROCHECK-NMR (34). Structure visualization was done with the program MOLMOL (35).

[2] The abbreviations used are: WT, wild type; r.m.s.d., root-mean-square deviation; NOE, nuclear Overhauser effect; NOESY, nuclear Overhauser enhancement spectroscopy; HSQC, heteronuclear single quantum coherence; MNK*n*, *n*th metal-binding domain of the human Menkes protein, ATP7A; DTT, dithiothreitol.

NMR Mobility Data Acquisition and Analysis—NMR experiments for determination of ^{15}N longitudinal and traverse relaxation rates (36) and $^{15}N\{^1H\}$ NOEs (37) were recorded at 298 K at 500 MHz using a protein concentration of 0.70 mM for both apo- and copper(I)-MNK3. R_1 and R_2 measurements for copper(I)-MNK3 were repeated also at 0.15 mM protein concentration. R_1 and R_2 relaxation rates were obtained by fitting the cross-peak volumes (I), measured as a function of the relaxation delay, to a single exponential decay by using the Levenberg-Marquardt algorithm as described in the literature (38). Uncertainties had been evaluated by using a Monte Carlo approach (38). Heteronuclear NOE values were calculated as the ratio of peak volumes in spectra recorded with and without saturation.

RESULTS

Protein Production—WT-MNK3 samples were not stable over a multi-day time frame and at the relatively high concentration needed for NMR. To improve the behavior of the protein, the K46V mutation was introduced. The rationale for introducing this particular mutation was based on both energetic considerations (obtained from the program PROSAII (39)) and on the inspection of multiple domain alignments, similar to what was done previously for *B. subtilis* CopA (40). The mutation was intended to make the folded form of MNK3 more compact, thus preventing the formation of insoluble aggregates. Introduction of a Val residue at position 46 resulted in a tighter packing of side chains at the exposed face of the β-sheet. K46V-MNK3 showed essentially the same spectral properties as WT-MNK3 and, in particular, essentially superimposable ^1H-^{15}N HSQC spectra (except for the mutated amino acid and immediate sequence neighbors). On the other hand, the stability of K46V-MNK3 was somewhat higher than that of WT-MNK3. Hereafter, we will refer to K46V-MNK3 as MNK3.

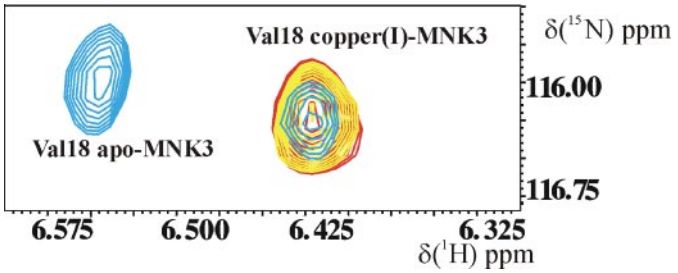

FIGURE 1. **Interaction of MNK3 with copper(I).** Superposition of a region of the ^1H-^{15}N HSQC NMR spectra of copper(I)-MNK3 (*red*), copper(I)-MNK3 in the presence of 10 mM reduced glutathione (*yellow*), and copper(I)-MNK3 in the presence of 3.0 mM DTT (*blue*). In the latter case only, a second peak appears in a position corresponding to that of the same signal in apo-MNK3. This indicates that DTT removes copper(I) from the metal-binding site. The assignment of peaks is shown.

Metallation of MNK3 was carried out by adding $Cu(CH_3CN)_4^+$ to solutions of the apoprotein reduced with DTT after removal of the reductant by means of a desalting column. DTT at millimolar concentration removed copper(I) from the metal-binding site of MNK3 (Fig. 1). This was at variance with what was observed for the other metal-binding domains of the Menkes protein (26), where there was no observable effect of DTT on copper(I)-binding by the protein. 10 mM glutathione, which is close to what is present *in vivo*, did not interfere with metal binding by MNK3 (Fig. 1). MNK3 could be metallated by an excess of copper(I)-HAH1 (Fig. 2). The ratio of the integrals of selected well resolved signals from apo- and copper(I)-MNK3 examined at various MNK3:HAH1 ratios allowed us to estimate an equilibrium constant for the metal transfer process from the metallochaperone to MNK3 of 0.06 ± 0.03, indicating that HAH1 actually has a higher affinity for copper(I) than MNK3. This equilibrium constant compares with values ranging between 5 and 10 for the other Menkes domains (26, 27).

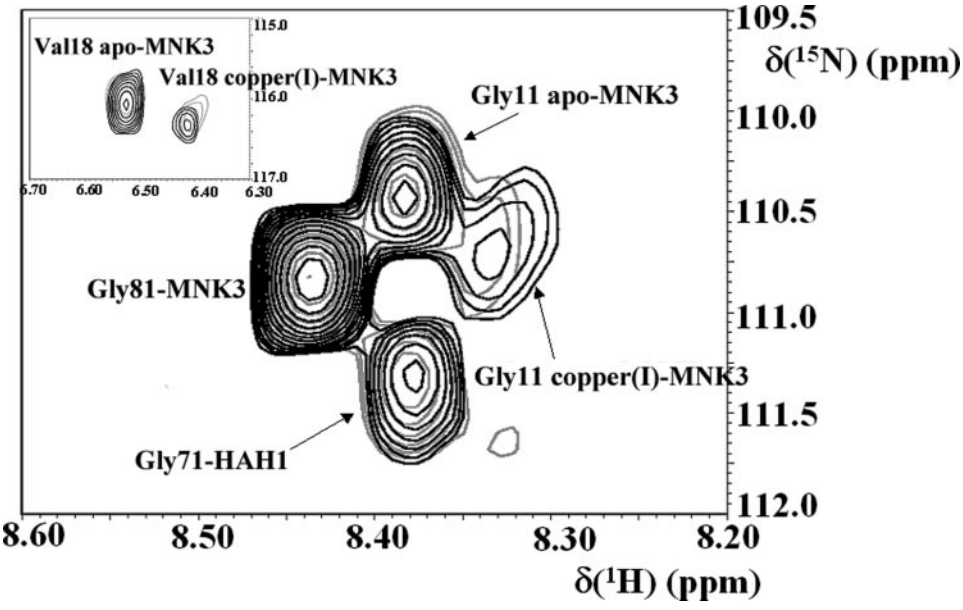

FIGURE 2. **Copper(I) transfer from HAH1 to MNK3.** Superposition of selected peak regions of the ^1H-^{15}N HSQC NMR spectra of apo-MNK3 in the presence of 2 equivalents of copper(I)-Hah1 (*gray*) and of 3 equivalent of copper(I)-Hah1 (*black*). Residues 81 of MNK3 and 71 of HAH1 are not affected by the presence of copper(I) and thus serve as an internal reference level.

NMR Spectroscopy and Structure Determination—In this work we applied automated methods for structure calculation based on the ATNOS/CANDID package (29, 30) for NOESY peak picking and assignment. The assigned NOE signals are converted to upper distance constraints and combined with the other constraints in the input for structure calculations. After restrained energy minimization with the AMBER 8.0 program, the final bundle of 30 conformers of apo-MNK3 had an average (over all conformers) for the target function of 0.89 ± 0.02 Å^2 (CYANA units), and the corresponding value for the copper(I)-MNK3 bundle of 30 conformers was 0.88 ± 0.03 Å^2. The average backbone r.m.s.d. values (over residues 2–75) for the apo- and copper(I)-

TABLE 1
Statistical analysis of the energy-minimized structures of apo- and copper(I)-MNK3

	Apo-MNK3	Copper(I)-MNK3
No. of meaningful constraints for each class		
Total number of NOE upper distance limits	1456	1047
Intra-residue	341	313
Inter-residue		
Sequential ($\|i-j\|=1$)	400	306
Medium range ($\|i-j\|\leq 4$)	246	130
Long range ($\|i-j\|\geq 5$)	469	298
Total dihedral angle restraints	134	143
Phi	40	47
Psi	94	96
r.m.s. violations per meaningful distance constraint (Å)[a]		
Intra-residue	0.0178 ± 0.0032	0.0188 ± 0.0034
Sequential	0.0223 ± 0.0022	0.0269 ± 0.0033
Medium range	0.0296 ± 0.0024	0.0290 ± 0.0073
Long range	0.0197 ± 0.0020	0.0347 ± 0.0030
r.m.s. violations per meaningful dihedral angle constraints (°)		
Phi	1.2655 ± 1.0035	2.0898 ± 0.8823
Psi	1.6509 ± 1.2182	2.9634 ± 2.1525
Average number of constraints per residue	18	13
Average number of violations per conformer		
Phi	1.40 ± 0.84	2.53 ± 1.26
Psi	1.37 ± 0.91	1.47 ± 0.99
NOE violations between 0.1 and 0.3 Å	20.5 ± 3.70	25.4 ± 4.80
NOE violations larger than 0.3 Å	0.000 ± 0.00	0.233 ± 0.20
Average r.m.s.d. to the mean (Å)[b]		
Backbone	0.49 ± 0.08	0.71 ± 0.12
Heavy	0.92 ± 0.08	1.14 ± 0.13
Structural analysis[c]		
% of residues in most favorable regions	77.9	72.8
% of residues in allowed regions	20.0	23.6
% of residues in generously allowed regions	1.3	2.7
% of residues in disallowed regions	0.9	0.9

[a] The data are calculated over the 30 conformers representing the NMR structure. The mean value and the standard deviation are given.
[b] The r.m.s.d. to the mean coordinates of the two bundles of 30 conformers was calculated for the backbone atoms N, C^{α}, C′ of residues 2–75.
[c] As it results from the Ramachandran plot analysis performed with PROCHECK.

MNK3 structures were, respectively, 0.51 ± 0.07 Å and 0.75 ± 0.13 Å; the all heavy atoms r.m.s.d. values are, respectively, 0.92 ± 0.06 Å and 1.22 ± 0.15 Å. Per residue r.m.s.d. values are shown in supplemental Fig. S1 for apo and copper(I)-MNK3. Table 1 reports some statistics on constraint violations in the final families, together with selected quality parameters from a PROCHECK-NMR (34) analysis. These data indicate that the solution structures obtained for both apo- and copper(I)-MNK3 are of good quality. Fig. 3 shows a comparison of the two structures. It can be seen that the largest structural changes upon metal binding occur in the loop regions, including the metal-binding loop, and at the domain termini. In addition, helix α1, which immediately follows the metal-binding loop, is shorter in copper(I)- than in apo-MNK3.

The dynamic properties of apo-MNK3 and copper(I)-MNK3 have been directly sampled through ^{15}N relaxation measurements (41). When comparing relaxation data at 0.7 mM concentration, there is no clear trend in the variation of R_1 rates between the two forms, whereas the R_2 rates in copper(I)-MNK3 are slightly higher than in apo-MNK3 all over the protein sequence (Fig. 4). Similar to the R_1 rates, the difference of $^{15}N\{^1H\}$NOEs between copper(I)- and apo-MNK3 does not show a significant trend (supplemental Fig. S2). These data suggest that upon metal binding, MNK3 experiences more pronounced conformational exchange equilibria than in the apo form. To rule out possible nonspecific protein aggregation in copper(I)-MNK3, leading to a generalized increase of R_2, we repeated the measurements after 5-fold dilution and found no significant change (within experimental error) in the ^{15}N relaxation rates (supplemental Figs. S3 and S4).

DISCUSSION

The third metal-binding domain of the human Menkes protein (ATP7A) has been overexpressed and subjected to NMR structural studies in both the apo- and copper(I)-loaded forms. The overall fold of the protein was unaffected by copper(I) binding, as observed previously for all other ATP7A domains (27, 28). However, the conformation of the metal-binding loop and of its neighboring residues was significantly affected by the presence of the metal ion. Indeed, it was observed that helix α1 is particularly long in apo-MNK3 with respect to the other ATP7A domains, starting from the residue preceding the second (in sequence) metal-binding cysteine. To bind the metal ion, the loop conformation then must rearrange in order to allow the side chains of the two cysteines to achieve the appropriate coordination geometry; this results also in partial unwinding of the helix α1, which is confirmed by the disappearance of the corresponding NOE pattern. In addition, at the other end of the metal-binding loop, the structural rearrangement upon metal binding causes a shortening also of the β-strand preceding the loop (β1). This results also in the shortening of strand β4, which faces β1 (Fig. 2). These effects are also associated with some enhancement in protein mobility, which can be related to the onset of chemical equilibria involving different conformations for the protein backbone. These equilib-

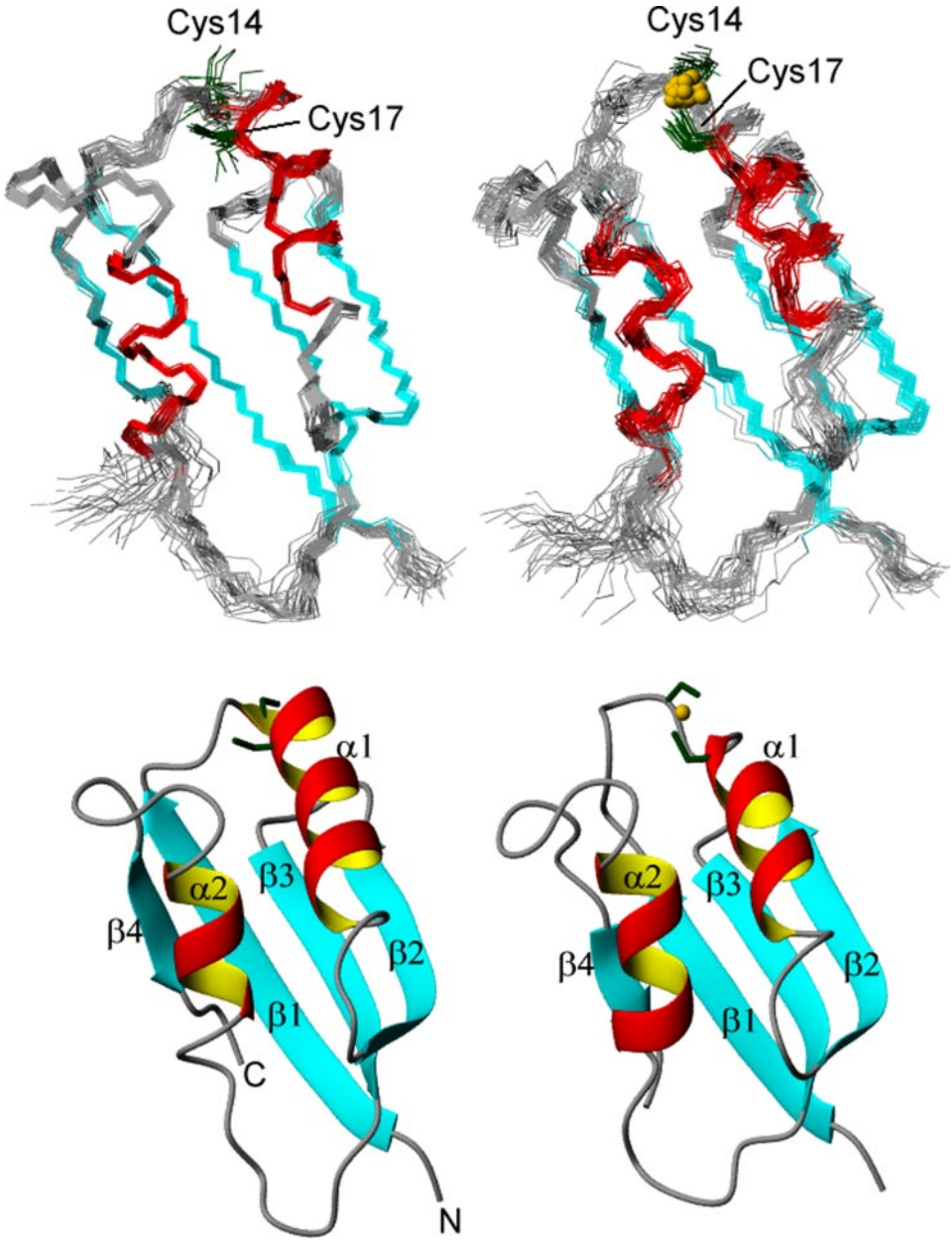

FIGURE 3. **Solution structures of apo- and copper(I)-MNK3.** *Top*, overlay of 30 conformers of the apo- (*left*) and copper(I)-MNK3 (*right*). Residues in helical conformation have been colored in *red*, and those in β-sheets are in *cyan*. The side chains of the copper(I)-binding cysteines (*dark green*) and the metal ion for copper(I)-MNK3 (*gold sphere*) are also shown. *Bottom*, ribbon representation of the average solution structure. The N and C termini and secondary structure elements are labeled.

ria could also be partly responsible for the lower number of NOEs detected for copper(I)-MNK3 when compared with apo-MNK3. Comparison of apo-MNK3 with *Enterococcus hirae* apo-CopZ (13) reveals a close coincidence of the polypeptide fold, similar to what has been found for other proteins and domains of these two classes. Residues 4–66 and 70–75 of MNK3 can be superimposed onto residues 1–62 and 63–68, respectively, of *E. hirae* CopZ (1–68) with a global r.m.s.d. value of 1.8 Å calculated for the backbone heavy atoms, although the sequence identity is only 25%. Furthermore, in both proteins the binding of Cu(I) leads to increased disorder, albeit without greatly affecting the global fold. An apparent difference in the behavior of the two proteins upon interaction with Cu(I) is that CopZ shows a tendency of self-aggregation (13), whereas there is no indication of Cu(I)-induced aggregation in MNK3.

The lower affinity of MNK3 for copper(I), highlighted by the inhibitory effect of DTT on metal binding (Fig. 1) and by the unfavorable thermodynamics of metal transfer from HAH1 (Fig. 2), seems to be the result of the energetically unfavorable reduction of the percentage of residues in regular secondary structure elements that takes place in concert with the necessary conformational rearrangement of the metal-binding loop. This effect proved destabilizing for the entire structure, as suggested by the analysis of protein dynamics (see above). MNK3 accepts copper(I) from its physiological partner, HAH1, without detectable formation of a metal-bridged adduct, as has been observed for the yeast homologous systems (20) or for the fourth domain of the ATP7B protein (42). Binding of the copper(I) ion by HAH1 is tighter than by MNK3 (Fig. 2), as indicted by the low value of the equilibrium constant for the transfer process.

If the amino acid sequences of the six metal-binding domains of ATP7A are aligned, it is found that MNK3 features the lowest similarity to the other five domains (12). When inspecting the sequences of the various ATP7A homologs across various mammalian organisms, it can be observed that the third domains are closest in sequence to one another. In particular, in the loop that precedes the last β-strand and is in contact with the metal-binding loop, Phe, which is conserved in all other domains, is substituted by Pro-66.

The sequence position of Pro-66 corresponds to the C terminus of helix α2 in the homologous proteins, which typically comprises residues 54–65 (numbering of the present protein). The occurrence of Pro-66 makes the helix shorter (because the Pro lacks the amide proton to form a hydrogen bond with the carbonyl oxygen of residue 62). As an example, Fig. 5 shows a superposition of MNK3 and MNK6. In the other ATP7A domains, it is found that Phe-66 is part of a network of hydrophobic contacts involving also the conserved Met located two residues before the metal-binding loop, the second metal-binding Cys, and a conserved Leu in loop III (27, 28). This core is

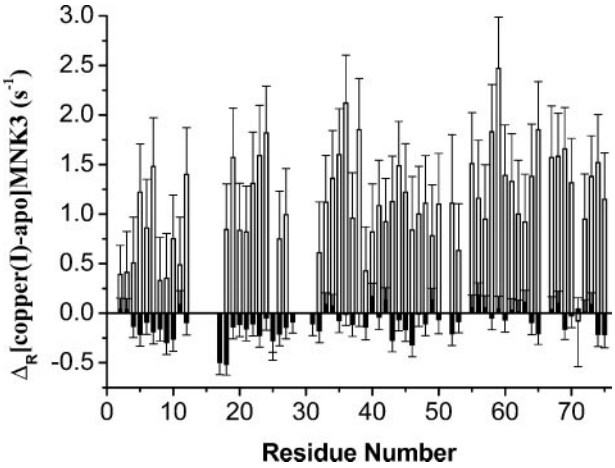

FIGURE 4. **^{15}N relaxation data for apo- and copper(I)-MNK3.** The difference between the ^{15}N relaxation rates of copper(I)- and apo-MNK3 is shown. *Black columns*, R_1 rates; *white columns*, R_2 rates.

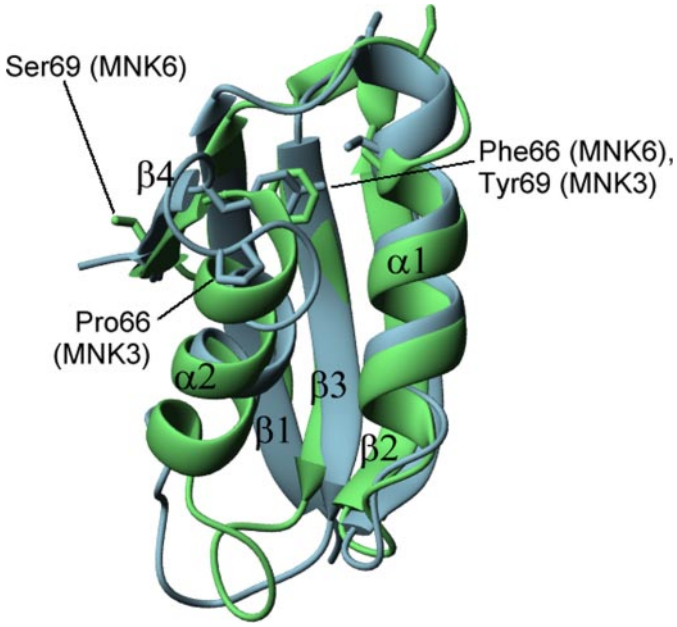

FIGURE 5. **Overlay of apo-MNK3 (*blue*) and apo-MNK6 (*green*).** The side chains of residues 66 and 69 are shown as *stick* diagrams for apo-MNK3 and apo-MNK6. Note that the numbering of residues in MNK6 has been offset by −1 with respect to what was used in the article reporting its structure (27), to make it consistent with the numbering used here for MNK3 and also for the majority of other MNK domains. Regular secondary structure elements are labeled.

present also in MNK3, where Tyr-69 plays the role of the missing Phe even though it is located three positions closer to the C terminus. In the other ATP7A domains, residue 69 is quite variable but always constitutes the second residue in the last strand of the β-sheet (β4). This is true even for the second domain, where there is a Phe at this position, in which the side chain is forcedly solvent-exposed to permit formation of the β-strand (28). Instead, in MNK3 the energetic driving force for formation of the hydrophobic core behind the metal-binding loop, which requires the participation of the side chain of Tyr-69, is such that the backbone of Tyr-69 cannot position itself to be part of the β-sheet (Fig. 5). The loop between helix α2 and strand β4 (loop V) is thus particularly long, as the helix is shorter than in the other domains and the strand is shifted toward the C terminus of the sequence, making its structure quite different from what is observed in all other ATP7A domains. Notably, predictions of domain boundaries based on multiple domain sequence alignments (12) locate the C terminus of the MNK3 domain within strand β4 rather than after its end, because of the shift of this strand along the sequence. Notwithstanding its small size, strand β4 appears to be particularly important with respect to the stability of the entire domain structure. In fact, in human MNK6 a mutation within this strand causes a destabilization of the β-sheet, resulting in enhanced solvent accessibility of the protein backbone and higher sensitivity to the presence of denaturants, which might contribute to the onset of Menkes disease (27).

In conclusion, MNK3 presents several unexpected peculiarities with respect to the other five domains of ATP7A, which have been structurally characterized already (26–28, 43–45). These differences are likely caused by the differences in sequence that are characteristics of the third domain. The structure, the dynamics, and the metal-binding properties of the protein are all affected, making MNK3 the worst site within the cytoplasmic tail of ATP7A for receiving copper(I) from the physiological partner. In the context of the entire ATP7A protein, metal binding is known to affect interdomain contacts, providing a possible mechanism to trigger ATP7A relocalization from the trans-Golgi network to the plasma membrane in the presence of excess copper (23, 25, 46). The unique features of MNK3, which are maintained in all mammalian homologs of human ATP7A, may constitute a further contribution to tuning this mechanism. Given its comparatively low affinity for copper(I), on thermodynamic grounds MNK3 would be the last domain to be metallated (note that the presence of glutathione at a concentration around physiological values did not prevent copper(I) binding, indicating that MNK3 can be metallated *in vivo*). Metallation of MNK3 could thus be an event quite suited to signal high intracellular copper(I) concentration and could trigger the appropriate response(s).

REFERENCES

1. Linder, M. C. (1991) *Biochemistry of Copper*, Plenum Press, New York
2. Vulpe, C. D., and Packman, S. (1995) *Annu. Rev. Nutr.* **15,** 293–322
3. O'Halloran, T. V., and Culotta, V. C. (2000) *J. Biol. Chem.* **275,** 25057–25060
4. Harrison, M. D., Jones, C. E., Solioz, M., and Dameron, C. T. (2000) *Trends Biochem. Sci* **25,** 29–32
5. Puig, S., and Thiele, D. J. (2002) *Curr. Opin. Chem. Biol.* **6,** 171–180
6. Huffman, D. L., and O'Halloran, T. V. (2000) *J. Biol. Chem.* **275,** 18611–18614
7. Rae, T., Schmidt, P. J., Pufahl, R. A., Culotta, V. C., and O'Halloran, T. V. (1999) *Science* **284,** 805–808
8. Klomp, L. W., Lin, S. J., Yuan, D., Klausner, R. D., Culotta, V. C., and Gitlin, J. D. (1997) *J. Biol. Chem.* **272,** 9221–9226
9. Pufahl, R. A., Singer, C. P., Peariso, K. L., Lin, S.-J., Schmidt, P. J., Fahrni, C. J., Cizewski Culotta, V., Penner-Hahn, J. E., and O'Halloran, T. V. (1997) *Science* **278,** 853–856
10. Petris, M. J., Mercer, J. F., Culvenor, J. G., Lockhart, P., and Camakaris, J. (1996) *EMBO J.* **15,** 6084–6095
11. Bull, P. C., and Cox, D. W. (1994) *Trends Genet.* **10,** 246–252
12. Arnesano, F., Banci, L., Bertini, I., Ciofi-Baffoni, S., Molteni, E., Huffman, D. L., and O'Halloran, T. V. (2002) *Genome Res.* **12,** 255–271
13. Wimmer, R., Herrmann, T., Solioz, M., and Wüthrich, K. (1999) *J. Biol.*

Chem. **274,** 22597–22603
14. Rosenzweig, A. C. (2001) *Acc. Chem. Res.* **34,** 119–128
15. Banci, L., and Rosato, A. (2003) *Acc. Chem. Res.* **36,** 215–221
16. Strausak, D., Howie, M. K., Firth, S. D., Schlicksupp, A., Pipkorn, R., Multhaup, G., and Mercer, J. F. (2003) *J. Biol. Chem.* **278,** 20821–20827
17. van Dongen, E. M., Klomp, L. W., and Merkx, M. (2004) *Biochem. Biophys. Res. Commun.* **323,** 789–795
18. Banci, L., Bertini, I., Ciofi-Baffoni, S., Del Conte, R., and Gonnelli, L. (2003) *Biochemistry* **42,** 1939–1949
19. Arnesano, F., Banci, L., Bertini, I., Cantini, F., Ciofi-Baffoni, S., Huffman, D. L., and O'Halloran, T. V. (2001) *J. Biol. Chem.* **276,** 41365–41376
20. Banci, L., Bertini, I., Cantini, F., Felli, I. C., Gonnelli, L., Hadjiliadis, N., Pierattelli, R., Rosato, A., and Voulgaris, P. (2006) *Nat. Chem. Biol.* **2,** 367–368
21. Goodyer, I. D., Jones, E. E., Monaco, A. P., and Francis, M. J. (1999) *Hum. Mol. Genet.* **8,** 1473–1478
22. Voskoboinik, I., Strausak, D., Greenough, M., Brooks, H., Petris, M., Smith, S., Mercer, J. F., and Camakaris, J. (1999) *J. Biol. Chem.* **274,** 22008–22012
23. Huster, D., and Lutsenko, S. (2003) *J. Biol. Chem.* **278,** 32212–32218
24. Walker, J. M., Huster, D., Ralle, M., Morgan, C. T., Blackburn, N. J., and Lutsenko, S. (2004) *J. Biol. Chem.* **279,** 15376–15384
25. Banci, L., Bertini, I., Cantini, F., Chasapis, C., Hadjiliadis, N., and Rosato, A. (2005) *J. Biol. Chem.* **280,** 38259–38263
26. Banci, L., Bertini, I., Chasapis, C., Ciofi-Baffoni, S., Hadjiliadis, N., and Rosato, A. (2005) *FEBS J.* **272,** 865–871
27. Banci, L., Bertini, I., Cantini, F., Migliardi, M., Rosato, A., and Wang, S. (2005) *J. Mol. Biol.* **352,** 409–417
28. Banci, L., Bertini, I., Del Conte, R., D'Onofrio, M., and Rosato, A. (2004) *Biochemistry* **43,** 3396–3403
29. Herrmann, T., Güntert, P., and Wüthrich, K. (2002) *J. Biomol. NMR* **24,** 171–189
30. Herrmann, T., Güntert, P., and Wüthrich, K. (2002) *J. Mol. Biol.* **319,** 209–227
31. Güntert, P., Mumenthaler, C., and Wüthrich, K. (1997) *J. Mol. Biol.* **273,** 283–298
32. Wishart, D. S., and Sykes, B. D. (1994) *J. Biomol. NMR* **4,** 171–180
33. Case, D. A., Darden, T. A., Cheatham, T. E., Simmerling, C. L., Wang, J., Duke, R. E., Luo, R., Merz, K. M., Wang, B., Pearlman, D. A., Crowley, M., Brozell, S., Tsui, V., Gohlke, H., Mongan, J., Hornak, V., Cui, G., Beroza, P., Schafmeister, C. E., Caldwell, J. W., Ross, W. S., and Kollman, P. A. (2004) *AMBER 8.0*, University of California, San Francisco
34. Laskowski, R. A., Rullmann, J. A. C., MacArthur, M. W., Kaptein, R., and Thornton, J. M. (1996) *J. Biomol. NMR* **8,** 477–486
35. Koradi, R., Billeter, M., and Wüthrich, K. (1996) *J. Mol. Graph.* **14,** 51–55
36. Farrow, N. A., Muhandiram, R., Singer, A. U., Pascal, S. M., Kay, C. M., Gish, G., Shoelson, S. E., Pawson, T., Forman-Kay, J. D., and Kay, L. E. (1994) *Biochemistry* **33,** 5984–6003
37. Grzesiek, S., and Bax, A. (1993) *J. Am. Chem. Soc.* **115,** 12593–12594
38. Mandel, M. A., Akke, M., and Palmer, A. G., III (1995) *J. Mol. Biol.* **246,** 144–163
39. Sippl, M. J. (1993) *Proteins Struct. Funct. Genet.* **17,** 355–362
40. Banci, L., Bertini, I., Ciofi-Baffoni, S., Gonnelli, L., and Su, X. C. (2003) *J. Mol. Biol.* **331,** 473–484
41. Ishima, R., and Torchia, D. A. (2000) *Nat. Struct. Biol.* **7,** 740–743
42. Achila, D., Banci, L., Bertini, I., Bunce, J., Ciofi-Baffoni, S., and Huffman, D. L. (2006) *Proc. Natl. Acad. Sci. U. S. A.* **103,** 5729–5734
43. Gitschier, J., Moffat, B., Reilly, D., Wood, W. I., and Fairbrother, W. J. (1998) *Nat. Struct. Biol.* **5,** 47–54
44. Jones, C. E., Daly, N. L., Cobine, P. A., Craik, D. J., and Dameron, C. T. (2003) *J. Struct. Biol.* **143,** 209–218
45. DeSilva, T. M., Veglia, G., and Opella, S. J. (2005) *Proteins* **61,** 1038–1049
46. Voskoboinik, I., Mar, J., Strausak, D., and Camakaris, J. (2001) *J. Biol. Chem.* **276,** 28620–28627

Solution Structure and Intermolecular Interactions of the Third Metal-binding Domain of ATP7A, the Menkes Disease Protein

Lucia Banci, Ivano Bertini, Francesca Cantini, Nunzia DellaMalva, Torsten Herrmann, Antonio Rosato and Kurt Wüthrich

J. Biol. Chem. 2006, 281:29141-29147.
doi: 10.1074/jbc.M603176200 originally published online July 26, 2006
